Biophysical Chemistry 138 (2008) 23–28

Contents lists available at ScienceDirect

Biophysical Chemistry

journal homepage: http://www.elsevier.com/locate/biophyschem

Sequence and stability of the goat cytochrome *c* ☆

Hamidur Rahaman [a], Khurshid Alam Khan [a], Imtaiyaz Hassan [a], Mohd. Wahid [a], S. Baskar Singh [b], Tej P. Singh [b], Ali Akbar Moosavi-Movahedi [c], Faizan Ahmad [a,*]

[a] Centre for Interdisciplinary Research in Basic Sciences, Jamia Millia Islamia, India
[b] Department of Biophysics, All India Institute of Medical Sciences, India
[c] Institute of Biochemistry and Biophysics, University of Tehran, Iran

ARTICLE INFO

Article history:
Received 14 July 2008
Received in revised form 20 August 2008
Accepted 22 August 2008
Available online 4 September 2008

Keywords:
Folding and stability
Molecular modeling
Goat cytochrome *c*
Bovine cytochrome *c*
Circular dichroism

ABSTRACT

We have determined the sequence of mitochondrial cytochrome *c* (cyt-*c*) from the goat heart, and it was found to have a unique amino acid sequence among all amino acid sequences of cyt-*c* reported till date. Its sequence alignment with the bovine cytochrome *c* (b-cyt-*c*) led us to conclude that the goat cytochrome *c* (g-cyt-*c*) differs in amino acid sequence from b-cyt-*c* at only one position, i.e., Pro44(bovine) → Ala44(goat). It has been observed that guanidinium chloride (GdmCl) induces a two-state transition between the native (N) and denatured (D) states of g-cyt-*c*. This conclusion is reached from the coincidence of GdmCl-induced transition curves monitored by measurements of absorbance at 405, 530 and 695 nm and circular dichroism (CD) at 222, 416 and 405 nm. Analysis of denaturation curves for the Gibbs energy of stabilization suggests that the stability of g-cyt-*c* is, within experimental errors, identical to that of b-cyt-*c*. We have also measured the effect of temperature on the equilibrium, N state ↔ D state of g-cyt-*c* in the presence of different GdmCl concentrations. These measurements gave values of transition temperature (T_m), changes in enthalpy (ΔH_m) and heat capacity (ΔC_p) of g-cyt-*c* in the absence of GdmCl, which are compared with those of b-cyt-*c*. We have used crystal structure coordinates of b-cyt-*c* to predict the structure and stability of g-cyt-*c*, which are compared with those of the bovine protein.

1. Introduction

The 'thermodynamic hypothesis' of Anfinsen [1] states that amino acid sequence determines protein conformation. Despite significant advancement that has been made toward the understanding of folding and stability of proteins, it is still not fully understood how the stabilization of protein is encoded in its sequence, and how individual amino acid residue contributes to the stability [2]. At present, site directed mutagenesis provides a powerful means of carrying out protein engineering as it enables the substitution of any constituent single residue or several residues at will [3]. Another convincing approach is a comparative study of the natural mutations on a protein that is available in different organisms of the same species. Cytochrome *c* (cyt-*c*) has been a model protein in the study of the evolution of protein sequence and structure. Since its evolution is more than 1.5 billion years, it has a large number of homologue natural mutants [4]. The homologue natural mutants are quite different in their sequence. Until now more than 200 mitochondrial cyt-*c* sequences have been reported [4–7] which does not include the one from the goat heart. In this study we report the sequence of mitochondrial cyt-*c* from the goat heart. Its sequence alignment with other homologue natural mutant revealed that the g-cyt-*c* has a unique sequence.

The effect of sequence variation on the folding and stability of few cyts-*c* has been reported earlier [8–10]. The solvent [8,10] and thermal [11,12] denaturation studies suggested that cyt-*c*, like most other single-domain protein in its size class (104 residues), exhibit a two-state equilibrium behavior. More recent spectroscopic study of the denaturation of two homologue natural mutants, horse cytochrome *c* (h-cyt-*c*) and bovine cytochrome *c* (b-cyt-*c*), which differ in three amino acid residues (Thr47(horse) → Ser47(bovine), Lys60 (horse) → Gly60(bovine) and Thr89(horse) → Gly89(bovine)) revealed that b-cyt-*c* is more stable than the h-cyt-*c*, and they follow different folding mechanisms [9]. To establish whether this difference in stability and mechanism of folding is due to variation in amino acid sequence, there is a need to study wide range of cyt-*c* from other sources. In this study we report our results of measurements of stability of g-cyt-*c* from guanidinium chloride (GdmCl)-induced denaturation followed by observing changes in the absorbance at 405, 530 and 695 nm and circular dichroism (CD) at 222, 405 and 416 nm. These results suggest that the stability of g-cyt-*c* is, within experimental errors, identical with that of the bovine cytochrome *c* (b-cyt-*c*), and its denaturation follows a two-state mechanism.

Abbreviations: ΔG_D^o, Gibbs energy change in the absence of denaturant; ΔG_s, solvation energy of chain folding; GdmCl, guanidinium chloride.

☆ Nucleotide sequence data of mitochondrial cytochrome *c* of the goat heart is available in the GenBank database under the accession number DQ176429.

* Corresponding author. Tel.: +91 11 26981733; fax: +91 11 26983409.
E-mail address: faizan_ahmad@yahoo.com (F. Ahmad).

0301-4622/$ – see front matter © 2008 Elsevier B.V. All rights reserved.
doi:10.1016/j.bpc.2008.08.008

Furthermore, to establish an exact relation between amino acid variations among species and structural stability, we have modeled the three dimensional (3D) structure of g-cyt-*c* based on the crystal structure of b-cyt-*c* [13]. These results are used to explain the observed stability of g-cyt-*c*.

2. Materials and methods

2.1. Materials

Amberlite CG-50 H^+ was available from HIMEDIA. Sephadex G-50 and CM-52 resin were from Sigma Chemical Co. (USA). An ultra pure GdmCl sample was purchased from MP Biomedicals, LLC (Aurora, Ohio, USA). Analytical grade sodium salt of cacodylic was purchased from the Sigma, and KCl was from Merck (India). These and other chemicals were analytical grade reagents and were used without further purifications.

2.2. Determination of amino acid sequence of goat cytochrome c

The amino acid sequence of cytochrome *c* from the goat heart was determined using the cDNA method. Total RNA from the goat heart was isolated by the phenol/chloroform method [14]. The poly A^+ RNA is isolated from the total RNA using oligo (dT) cellulose column (Stratagene, USA). The full-length ds cDNA synthesis was carried out using MarathonT-cDNA amplification kit (Clontech, USA) as per the manufacturer's protocol. PCR reactions were performed with the cDNA, using 5-GGT GAT GTT GAR AAR GGC AAG-3 as forward primer and 5-TTA CTC ATT RGT AGC TTT TTT SAG-3 as reverse primer. These primers were designed after comparing the cyt-*c* of the other mammals available in the GenBank. The resulted 315 bp of PCR amplified product was cut and eluted with gel elution kit (Qiagen, Germany). This eluted product of g-cyt-*c* was cloned in pGEMT-easy vector (Promega). One positive clone was selected for DNA sequencing (ABI Prism 3730) using T7 primer. The complete nucleotide sequence has already been deposited in the GenBank (Accession number DQ176429).

2.3. Isolation and purification of cyt-c from the goat heart

The cyt-*c* was isolated from the goat heart by the method published by Margoliash and co-workers [15,16]. The goat heart was weighed prior to homogenization so that the yield per gram can be determined. Coarse filter paper was used for filtration of the initial extract. Amberlite CG-50 was used for the first ion-exchange chromatography while CM-52 cellulose serves as the resin for the second and third ion-exchange chromatography steps. The sample was concentrated by ultrafiltration prior to gel filtration using YM3 membranes, which have a molecular weight cut-off of 3000. There are different forms of cyt-*c*, which may not be completely separated by this procedure. As deamidated forms of cyt-*c* elute prior to the native cyt-*c* [16], a UV-detector can be used for the final ion-exchange step since that steps separates different forms of cyt-*c* from each other. The gel filtration step used a column (1.5×30 cm) with a flow rate of 30 mL/h. Finally desalting and concentration was accomplished using ultrafiltration YM3 membranes (Amicon Corporation, USA). The yield of cyt-*c* was 18 μmol/kg.

The protein was characterized for purity, size and spectral properties. UV–visible spectroscopy from 240 to 700 nm was used to show that the red protein isolated was indeed cyt-*c*. Spectra of both oxidized and reduced cyt-*c* were collected and compared with published spectra to determine that the proper changes in absorbance occur as the oxidation state of the protein changes [15]. SDS-PAGE was used to access the purity of the isolated cyt-*c*. It gave a single band of protein with a molecular weight of about 12,400 (Fig. 1).

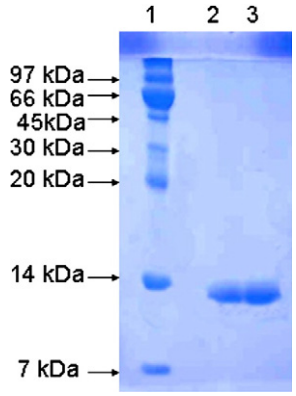

Fig. 1. SDS-PAGE of g-cyt-*c*. Lane 1 was loaded with 2.7 μg of polypeptide markers. Lanes 2 and 3 were loaded with 2.7 μg of h- and g-cyts-*c*.

2.4. Measurements of denaturation curves

The goat cytochrome *c* (g-cyt-*c*) was oxidized first by adding 0.1% potassium ferricyanide using a procedure described earlier [17] which ensures that the heme iron is completely in the Fe(III) state. The degree of oxidation was checked by measuring ε, the molar absorption coefficient, values at 550 and 360 nm at which oxidized and reduced forms have significantly different values of the optical parameter [18]. The concentration of the oxidized cyt-*c* was determined experimentally using a value of 106 000 M^{-1} cm^{-1} for ε at 409 nm [18]. For optical measurements all solutions were prepared in 0.03 M cacodylate buffer containing 0.1 M KCl at pH 6.0 and incubated overnight at room temperature.

Isothermal denaturation of cyt-*c* by GdmCl at 25.0±0.1 °C was measured in Shimadzu 2100 UV/Vis Spectrophotometer whose temperature was maintained by circulating water from an external thermostated bath and in Jasco J-715 Spectropolarimeter equipped with a Peltier-type temperature controller (PTC-348WI). Protein concentration used for the absorption measurements in the Soret and IR regions was in the range 7–10 μM and 80–85 μM, respectively, and 1 cm path length cells were used. For CD measurements in the far-UV and Soret regions, 0.1 and 1 cm path length cells were used respectively, and protein concentration was in the range 18–20 μM.

The thermal denaturation measurements of the protein in the presence and absence of different GdmCl concentrations were carried out in Jasco Spectropolarimeter, and in Jasco V-560 UV/Vis Spectrophotometer, also equipped with a peltier-type temperature controller (ETC-505T), with a heating rate of 1 °C/min. This scan rate was found to provide adequate time for equilibration.

The CD instrument was routinely calibrated with D-10-camphorsulphonic acid. The results of all the CD measurements are expressed as mean residue ellipticity ($[\theta]_\lambda$) in deg cm^2 $dmol^{-1}$ at a given wavelength λ (nm) using the relation:

$$[\theta]_\lambda = \theta_\lambda M_0 / 10cl \quad (1)$$

where θ_λ is the observed ellipticity in millidegrees at wavelength λ, M_0 is the mean residue weight of the protein, c is the protein concentration (mg/cm^3), and l is the path length (cm). It should be noted that each observed θ_λ of the protein was corrected for the contribution of the solvent. Reversibility of the isothermal denaturation by GdmCl was checked using the procedure described earlier [19]. At a given denaturant concentration point from the denaturation and renaturation experiments were measured and compared to check the reversibility. Reversibility of the thermal denaturation was checked by matching the optical properties before and after denaturation.

```
ggt gat gtt gag aag ggc aag aag att ttt gtt cag aag tgt gcc cag tgc cat act gtg    060
 G   D   V   E   K   G   K   K   I   F   V   Q   K   C   A   Q   C   H   T   V    020
gaa aag gga ggg aag cac aag act ggg cca aac ctc cat ggt ctg ttt gga cga aag aca    120
 E   K   G   G   K   H   K   T   G   P   N   L   H   G   L   F   G   R   K   T    040
ggt cag gct gct ggg ttt tct tac aca gat gcc aac aaa aac aaa ggt atc acc tgg gga    180
 G   Q   A   A   G   F   S   Y   T   D   A   N   K   N   K   G   I   T   W   G    060
gag gag acg ctg atg gag tac ttg gag aat ccc aag aag tac atc cct gga acc aaa atg    240
 E   E   T   L   M   E   Y   L   E   N   P   K   K   Y   I   P   G   T   K   M    080
atc ttt gct ggc att aag aag aag gga gag agg gag gac ttg ata gct tat ctc aaa aaa    300
I    F   A   G   I   K   K   K   G   E   R   E   D   L   I   A   Y   L   K   K    100
gct acc aat gag taa*                                                              312
A    T   N   E  Stop
```

Fig. 2. Nucleotide sequence and the deduced amino acid sequence of the g-cyt-*c*.

2.5. Model building and structure analysis

The crystal structure of b-cyt-*c* is already known [13]. Using COOT package from CCP4 suite [20] with the known coordinates of b-cyt-*c*, structure of the goat protein was generated. The generated structure of g-cyt-*c* was subjected to energy minimization in SwissPdbViewer software [21] for correcting its stereochemistry. The geometric inaccuracies of this predicted structure was further refined by submitting it to RCSB ADIT Validation server, an online web interface (http://deposit.pdb.org/validate/) which provides validation reports from PROCHECK [22] to ensure the sterochemical quality of coordinates. This server also checks whether all residues fall in the allowed regions of the Ramachandran plot [23]. The program PROCHECK verifies the parameters like bond length, bond angle, main chain and side chain properties, residue-by-residue properties, RMS distance from planarity and distorted geometry plots. The final refined coordinates of g-cyt-*c* along with the known coordinates of b-cyt-*c* were used to draw ribbon diagram using PyMol software [24]. To determine solvation energy of protein folding, coordinates of both proteins were submitted to an online server PISA provided by European Bioinformatics Institute (EBI) (http://www.ebi.ac.uk/msd-srv/prot_int/pistart.html).

3. Results

3.1. Amino acid sequence

The amino acid sequence of the mitochondrial cyt-*c* from the goat heart has been determined using cDNA method [25]. The nucleotide deduced amino acid sequence of g-cyt-*c* is shown in Fig. 2. The amino acid sequence alignment of g-cyt-*c* with amino acid sequences of all mitochondrial cyts-*c* available at NCBI sequence database revealed that it has a unique sequence. Its alignment with the most studied mitochondrial cyt-*c* from the bovine (sequence not shown) led us to conclude that the goat cytochrome *c* (g-cyt-*c*) differs in amino acid sequence from b-cyt-*c* at only one position, i.e., Pro44(bovine) → Ala44(goat).

3.2. Isothermal denaturation of g-cyt-c by GdmCl

GdmCl-induced unfolding transitions of g-cyt-*c* were monitored by $\Delta\varepsilon_{405}$, $\Delta\varepsilon_{530}$ and $[\theta]_{405}$ (probes for measuring the change in the heme–globin interaction), $\Delta\varepsilon_{695}$ (probe for measuring the change in the heme–Met80 interaction), $[\theta]_{222}$ (probe for measuring change in the backbone conformation), and $[\theta]_{416}$ (probe for measuring change in the heme–methionine environment). Unfolding transitions of the protein were found reversible over the entire concentration range of the denaturant. Using a non-linear least-squares method, the entire ($y(g)$, [g]) data of each denaturant-induced transition curve (e.g., see insets in Fig. 4) were analyzed for ΔG^{o}_{D} and m_g using the relation [26]:

$$y(g) = y_N(g) + y_D(g) \times Exp\left[-(\Delta G^{o}_{D} + m_g[g])/RT\right]/(1 + Exp\left[-(\Delta G^{o}_{D} + m_g[g])/RT\right]) \quad (2)$$

where $y(g)$ is the observed optical property at [g], the molar concentration of GdmCl, $y_N(g)$ and $y_D(g)$ are optical properties of the native and denatured protein molecules under the same experimental conditions in which $y(g)$ was measured, ΔG^{o}_{D} is the value of Gibbs energy change (ΔG_D) in the absence of the denaturant, m_g is the slope ($\partial\Delta G_D/\partial[g]$), R is the universal gas constant, and T is the temperature in Kelvin. The values of ΔG^{o}_{D}, m_g and C_m ($=\Delta G^{o}_{D}/m_g$) of GdmCl-induced denaturation of g-cyt-*c* are given in Table 1. This table also shows values of these stability parameters of cyt-*c* from the bovine [9]. It should, however, be noted that the analysis of each GdmCl-induced transition curve was done assuming that unfolding is a two-state process, and [g]-dependencies of $y_N(g)$ and $y_D(g)$ are linear (i.e., $y_N(g) = a_N + a_N[g]$ and $y_D(g) = a_D + b_D[g]$, where a and b are [g]-independent parameters, and subscripts N and D represent these parameters for the native and denatured protein molecules, respectively). Values of a_N, b_N, a_D and b_D are not shown here. Fig. 3 shows the normalized transition curves of GdmCl-induced denaturation of g-cyt-*c*. In this figure, $f_d = (y(g) - a_N - b_N[g])/(a_D + b_D[g] - y(g))$ is the fraction of denatured protein molecules at a given [g]. Since all data points from different optical probes fall on the same normalized curve (see Fig. 3), these results suggest that the GdmCl-induced denaturation of g-cyt-*c* is a two-state process.

Table 1
Thermodynamic and conformational parameters associated with GdmCl-induced denaturation of g-cyt-*c* and b-cyt-*c* at pH 6.0 and 25±0.1 °C[a]

Probe	g-cyt-*c*			b-cyt-*c*[b]		
	ΔG^{o}_{D} (kJ mol^{-1})	m_g (kJ mol^{-1}[g]$^{-1}$)	C_m (M)	ΔG^{o}_{D} (kJ mol^{-1})	m_g (kJ mol^{-1}[g]$^{-1}$)	C_m (M)
$[\theta]_{222}$	38.9±1.7	−15.5±0.8	2.5±0.2	44.7±1.3	−16.8±0.5	2.6±0.4
$[\theta]_{405}$	40.1±2.9	−15.5±1.3	2.6±0.3	42.7±1.3	−16.4±0.8	2.6±0.2
$[\theta]_{416}$	38.9±1.7	−15.5±0.8	2.5±0.2	44.1±1.3	−16.9±1.1	2.6±0.2
$\Delta\varepsilon_{405}$	39.7±3.8	−15.0±0.4	2.7±0.3	43.3±0.3	−16.4±0.8	2.7±0.2
$\Delta\varepsilon_{695}$	40.9±2.1	−15.5±0.8	2.7±0.8	44.7±3.5	−16.8±1.3	2.7±0.3
$\Delta\varepsilon_{530}$	39.3±2.5	−15.0±1.2	2.6±0.3	43.9±2.3	−16.5±0.8	2.7±0.4

[a] A±with each parameter represents an error from the mean of errors from the triplicate measurements. It should be noted that the standard errors in the estimation of a thermodynamic parameter by fitting a set of data to Eq. (2) is less than the mean error from independent measurements.
[b] Data taken from [9].

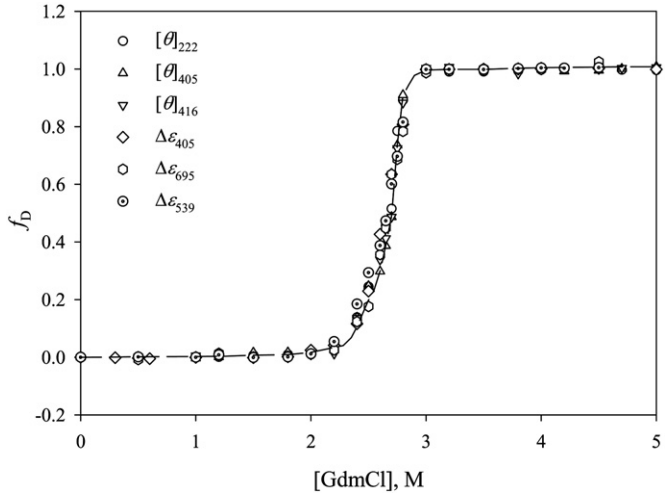

Fig. 3. GdmCl-induced denaturation of g-cyt-*c* at pH 6.0 and 25±0.1 °C. Plot of f_D versus [GdmCl].

3.3. Effect of temperature on the equilibrium, N state ↔ D state

Heat-induced denaturation of g-cyt-*c* in the presence of various concentrations of GdmCl was measured at pH 6.0, and a total of about 500 data points were collected for each transition curve. It has been observed that the thermal denaturation of g-cyt-*c* in the presence of GdmCl is reversible. Fig. 4A shows the heat-induced denaturation curves of the protein measured by observing changes in $\Delta\varepsilon_{405}$ in the presence of different concentrations of GdmCl. It has been observed that $\Delta\varepsilon_{405}$ of the protein in the native and denatured states show dependence on both [*g*] and temperature. These dependencies of y_N and y_D on both [*g*] and temperature are given by the following equations:

$$y_N = -145.4(\pm 10.6)T + 3914.9(\pm 189.7)[g] + 2183.8(\pm 174.5) \quad (3)$$

$$y_D = -133.2(\pm 3.9)T + 4090.9(\pm 350.5)[g] + 30820.6(\pm 1629.8) \quad (4)$$

It should be noted that for the protein, the dependence of y_D on the composition variables ([*g*] and *T*) was determined from the analysis of the temperature-dependence of all $\Delta\varepsilon_{405}$ data at each [*g*] in the range

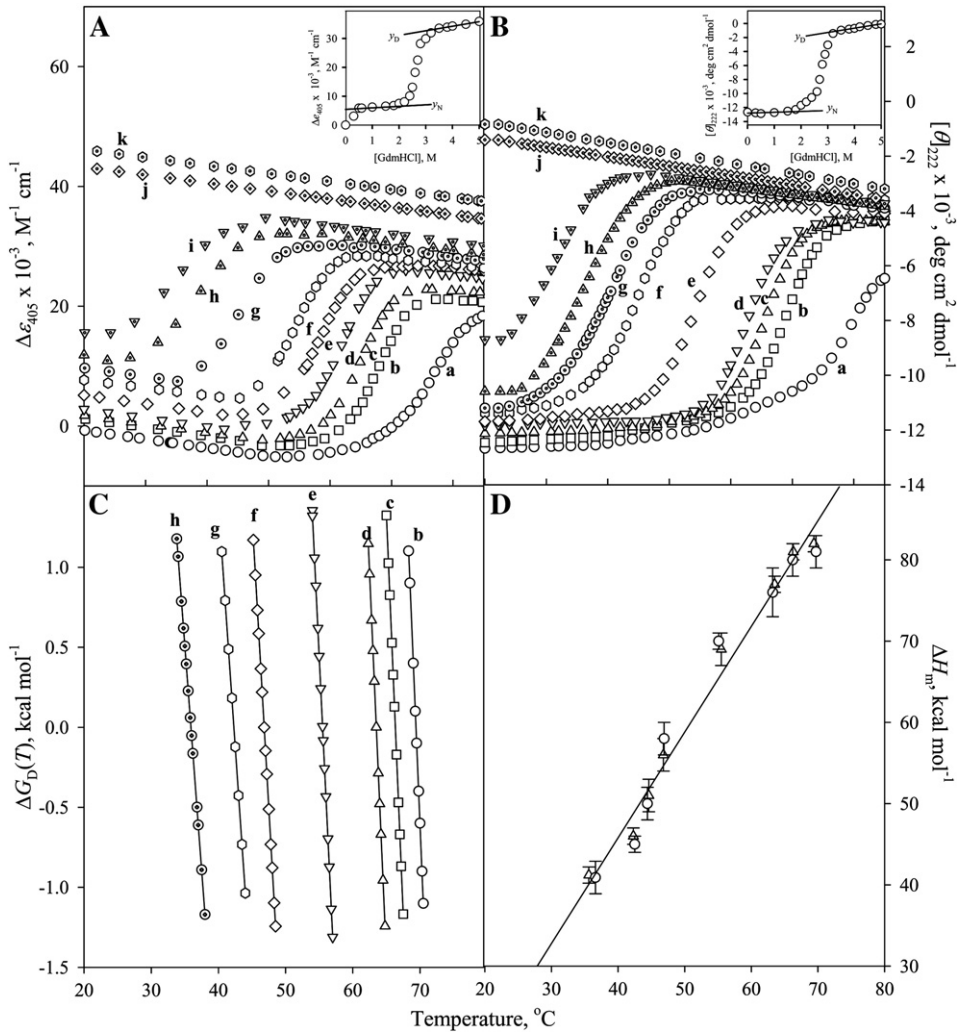

Fig. 4. Temperature dependence of properties of g-cyt-*c* at pH 6.0. (A) Effect of temperature on the GdmCl-induced denaturation monitored by $\Delta\varepsilon_{405}$: a, 0 M; b, 0.6 M; c, 0.8 M; d, 1.0 M; e, 1.5 M; f, 2.0 M; g, 2.2 M; h, 2.4 M; i, 2.5 M; j, 3.5 M; and k, 4.5 M GdmCl. (B) Effect of temperature on the GdmCl-induced denaturation monitored by $[\theta]_{222}$: curves numbers have the same meaning as in A. (C) Stability curves of the protein at different GdmCl concentrations, where curve numbers have the same meaning as in A and B. (D) Plots of ΔH_m versus T_m: (ΔH_m, T_m) data determined from $\Delta\varepsilon_{405}$ (o) and $[\theta]_{222}$ (Δ) measurements. The errors in T_m are not shown, for the error bars are smaller than the symbols used. In order to maintain clarity all data points are not shown in A and B.

Table 2
Thermodynamic parameters associated with N state ↔ D state of g-cyt-*c* in the presence of different concentrations of GdmCl at pH 6.0[a]

	$\Delta\varepsilon_{405}$		$[\theta]_{222}$	
[d]	ΔH_m^{Van}	T_m	ΔH_m^{Van}	T_m
(M)	(kJ mol^{-1})	(°C)	(kJ mol^{-1})	(°C)
0.6	338.6±8.3	69.7±0.2	342.8±4.2	69.4±0.1
0.8	334.4±8.3	66.2±0.1	338.6±4.2	66.3±0.3
1.0	317.7±12.5	63.2±0.2	321.9±4.2	63.5±0.1
1.5	292.2±4.2	55.1±0.5	288.4±8.3	55.5±0.3
2.0	242.4±8.3	46.9±0.5	234.1±8.3	46.8±0.2
2.2	209.0±8.3	44.4±0.6	213.2±8.3	44.6±0.1
2.3	188.1±4.2	42.5±0.4	199.2±8.3	42.3±0.1
2.5	171.4±8.3	36.6±0.5	175.6±4.2	35.6±0.2

[a] A±with each parameter has the same meaning as in Table 1.

2.4–4.5 M, whereas in determining the dependence of y_N on the composition variables only the pre-transition region data at each [*g*] in the concentration range 0–1.5 M were used. Furthermore, in Eqs. (3) and (4) y_N and y_D are in M^{-1} cm^{-1}, and *T* is in °C.

Fig. 4B shows the heat-induced denaturation of g-cyt-*c* in the presence of different concentrations of GdmCl at pH 6.0, monitored by observing changes in $[\theta]_{222}$. It has been observed that $[\theta]_{222}$ values of the native and denatured protein molecules show dependence on both temperature and [*g*]. These dependencies of $[\theta]_{222}$ (deg cm^2 dmol^{-1}) of the protein on the composition variables ([*g*] and *T*) were determined using data in the same [*g*] ranges as used in the case of $\Delta\varepsilon_{405}$ measurements. Relations describing these dependencies are given by the following equations:

$$y_N = 6.7(\pm0.4)T + 798.4(\pm96.9)[g] - 12822.8(\pm68.5) \quad (5)$$

$$y_D = [-5.1(\pm0.2)[g] - 15.8(0.8)]T + 669.9(\pm50.5)[g] - 2924.9(\pm123.9) \quad (6)$$

Assuming that heat-induced denaturation of a protein in the absence and presence of GdmCl follows a two-state mechanism at a given [*g*], values of ΔG_D as a function of temperature were estimated from each denaturation curve shown in Fig. 4A and B, using the relation:

$$\Delta G_D(T) = -RT\ln[(y(T) - y_N(T)/(y_D(T) - y(T)] \quad (7)$$

where *R* is the gas constant, $y(T)$ is the experimentally observed optical property of the protein at temperature *T* K, y_N and y_D are, respectively, the optical properties of the native and denatured protein molecules under the same experimental conditions in which $y(T)$ was measured. To construct stability curve values of ΔG_D (T) in the range $-5.4 \le \Delta G_D$ (T) (kJ mol^{-1})≤ 5.4 in the presence of various concentrations of GdmCl are plotted against temperature. Stability curves thus obtained from the CD measurements are shown in Fig. 4C. Each stability curve at a given [*g*] was analyzed to determine values of T_m and ΔH_m using the procedure described earlier [27]. These values of T_m and ΔH_m in the presence of GdmCl are given in Table 2. Stability curves obtained from absorption measurements (see Fig. 4A) were also constructed (stability curves not shown). These curves were also analyzed for ΔH_m and T_m, and these values are given in Table 2. It is seen in this table that each of the thermodynamic property obtained from two quite different optical properties is, within experimental errors, identical. This agreement suggests that our assumption that the heat-induced denaturation of g-cyt-*c* in the presence of GdmCl is a two-state process seems to be valid.

Fig. 4D shows plot of ΔH_m and T_m of g-cyt-*c*. A linear least-square analysis was used to analyze this plot to determine ΔC_p, the constant-pressure heat capacity change $(=(\partial\Delta H_m/\partial T_m)_p)$. The value of ΔC_p thus obtained is 5.4±0.3 kJ mol^{-1} K^{-1}. We constructed plots of ΔH_m versus [*g*] and T_m versus [*g*] (not shown) using values of T_m and ΔH_m at different GdmCl concentrations given in Table 2. These plots were found linear. Using the linear least-squares analysis values of $\Delta H_m(0)$, the value of ΔH_m at 0 M GdmCl and $T_m(0)$, the value of T_m at 0 M GdmCl, were determined. These values are given in Table 3 and are compared with those of b-cyt-*c*.

The value of ΔG_D^o of g-cyt-*c* in the absence of GdmCl was estimated using Gibbs–Helmholtz equation with observed values of T_m (0), ΔH_m (0) and ΔC_p (Table 3):

$$\Delta G_D^o = [\Delta H_m(0)(T_m(0) - 298.15)/T_m(0))] - \Delta C_p[(T_m(0) - 298.15) + 298.15\ln(298.15/T_m(0))] \quad (8)$$

3.4. Structure analysis

Using procedures described in "Materials and methods" section, the energy minimized coordinates of g-cyt-*c* were determined in this study from the known atomic coordinates of b-cyt-*c* [13]. The C^α traces of both cyts-*c* are superimposed in Fig. 5. It is seen in this figure that due to high sequence similarity there is minimal RMS deviations. This structural analysis also reveals that all contacts made by Pro44 in b-cyt-*c* (or Ala44 in g-cyt-*c*) are parts of the main chain C^α atoms, and no contacts are made by the side chain atoms. Fig. 5 also shows all the possible hydrogen bonds. It should be noted that, in addition to these bondings, there exists one van der Waals interaction between Pro44C^δ and Gln42O, which is not present in the goat protein.

Table 3
Thermodynamic parameters associated with N state ↔ D state transition of cyts-*c* in absence of GdmCl at pH 6.0[a]

Parameters	g-cyt-*c*	b-cyt-*c*[b]
ΔG_D^0 (kJ mol^{-1})	38.5±2.5 (39.7±2.5)	40.1±0.8 (43.9±1.7)
$\Delta H_m(0)$ (kJ mol^{-1})	409.6±13.4	418.0±12.1
$T_m(0)$ (°C)	79±0.3	80±0.2
ΔC_p (kJ mol^{-1} K^{-1})	5.4±0.37	5.1±0.2

[a] Values in parenthesis were determined from the isothermal GdmCl-induced denaturation at pH 6.0 and 25±0.1 °C.
[b] Data taken from [9].

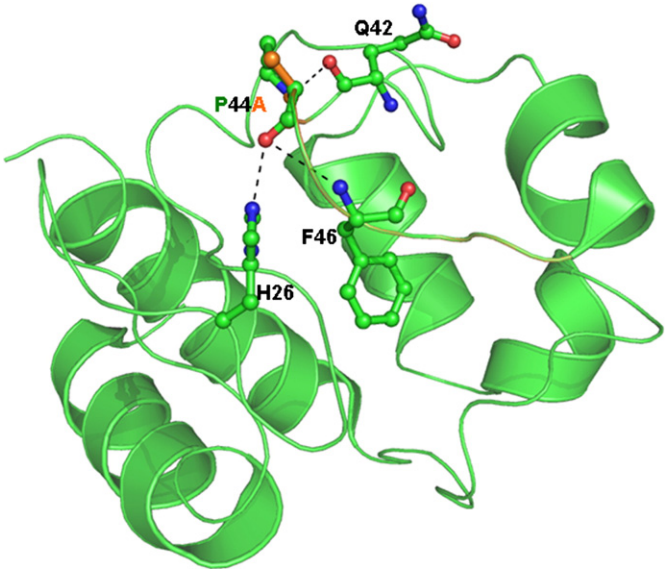

Fig. 5. 3D structural comparison of b-cyt-*c* (green) and g-cyt-*c* (orange). Residue at positions at 26, 42, 44 and 46 are represented in ball and stick, and involvements in H-bond formations are also shown.

4. Discussion

In this study we have experimentally determined ΔG^{o}_{D} of g-cyt-*c* using two methods and compared it with that of b-cyt-*c*. The first method involves the measurements of GdmCl-induced denaturation monitored by various optical probes at pH 6.0 and 25 °C (Fig. 3). Assuming a two-state transition denaturation mechanism (Fig. 3), all these transition curves were analyzed for ΔG^{o}_{D}, m_g and C_m which were compared with those of b-cyt-*c* (Table 1). It is seen in this table that the average value of each thermodynamic parameter of g-cyt-*c* is, within experimental errors, identical to those obtained for b-cyt-*c* [9].

Secondly, ΔG^{o}_{D} values can also be determined using Eq. (8) if values of $\Delta H_m(0)$, $T_m(0)$ and ΔC_p are known. We have determined ΔH_m, T_m (Table 2), the values of thermodynamic parameters from the analysis of the heat-induced denaturation curves of g-cyt-*c* in the presence of different fixed concentrations of GdmCl (Fig. 4A and B) and a linear extrapolation of plots of ΔH_m versus [*g*] and T_m versus [*g*] to 0 M denaturant concentration gave $\Delta H_m(0)$ and $T_m(0)$ values (Table 3). We have determined the value of ΔC_p from the (ΔH_m, T_m) data given in Table 2. A least-squares analysis of the plot of ΔH_m versus T_m gave a value of 5.4±0.3 kJ mol^{-1} K^{-1} for ΔC_p. Using values of $\Delta H_m(0)$, T_m (0) and ΔC_p of g-cyt-*c* (Table 3) in Eq. (8), we estimated a value of 38.5± 2.5 kJ mol^{-1} for ΔG^{o}_{D}. This value is an excellent agreement with that (ΔG^{o}_{D}=39.7±2.5 kJ mol^{-1}) obtained from the isothermal GdmCl-induced denaturation curves of g-cyt-*c*. We conclude that Gibbs energy change associated with the g-cyt-*c* transition, N state ↔ D state is in the range 38.5–39.7 kJ mol^{-1} at pH 6.0 and 25 °C.

As we mentioned above, a single residue difference between sequences of g-cyt-*c* and b-cyt-*c* is at the position 44, and Pro44 of the bovine protein is exposed to the solvent. Table 3 compares values of thermodynamic parameters of g-cyt-*c* with those of b-cyt-*c*. It is seen in this table that all the thermodynamic parameters of the goat protein are, within experimental errors, identical to those of the bovine protein (for a comparison of thermodynamic data of cyts-*c* from the bovine and horse hearts, see Ref. [9]). This agreement suggests that the residue Ala44 of g-cyt-*c* is not only exposed to the solvent but also the substitution of Pro with Ala in b-cyt-*c* does not lead to change in the non-covalent interaction with the other residues of the protein. To see whether these are indeed true, we have determined the structure of g-cyt-*c* using published coordinates of b-cyt-*c*.

Knowing that g-cyt-*c* differs at the position 44 from that of b-cyt-*c*, we have generated the structural coordinates of g-cyt-*c* from the known coordinates of the bovine protein [13] using the simple mutate tool from COOT package of CCP4 suite. The theoretically generated structure of the backbone along with side chains at the position 44 is superimposed the structure of b-cyt-*c* in Fig. 5. This superimposition shows that there are minimal RMS deviations suggesting that both cyts-*c* have almost identical backbone configuration. Furthermore, we have also determined the non-covalent interaction between residue 44 and other residues in both proteins. This determination showed us that all interactions are between main chain atoms of Pro44 in b-cyt-*c* (or Ala44 in g-cyt-*c*) and none of the interactions are made by side chain atoms of the residue 44 in both proteins.

Eisenberg and McLachlan [28] developed a method for estimating solvation energy contribution to protein stability in water from its atomic coordinates. It should be noted that this method does not yield ΔG^{o}_{D} value of a protein rather it provides a solvation energy contribution to ΔG^{o}_{D}. However, this method is applicable to get relative stability of a protein in different conformations [28]. Using PISA server, we have estimated solvation free energy (ΔG_s) contributions to the overall stability of the goat cyt-*c* (ΔG_s=−365.3 kJ mol^{-1}) and bovine cyt-*c* (ΔG_s=−364.9 kJ mol^{-1}). An identical value for this parameter suggests that additional van der Waals interaction present in the bovine protein has no significant contribution to ΔG_s. Thus, the estimation of ΔG_s values and the structural analysis (almost identical conformation shown in Fig. 5) support our experimental finding that g-cyt-*c* and b-cyt-*c* have identical folding energy (ΔG^{o}_{D}).

Finally, our thermodynamic and structural analysis led us to conclude that the 3D structure of g-cyt-*c* will be almost identical to that of the bovine protein [13]. The 3D structural determination of the goat cytochrome *c* is already in progress in our lab.

Acknowledgements

This work supported by grants from the CSIR and DST to FA. MHR, MKAK, MW and MI H are thankful to the UGC, CSIR, ICMR and DST for the fellowships, respectively.

References

[1] C.B. Anfinsen, Principles that govern the folding of protein chains, Science 181 (1973) 223–230.
[2] K. Fan, W. Wang, What is the minimum number of letters required to fold a protein? J. Mol. Biol. 328 (2003) 921–926.
[3] W. Colon, G.A. Elove, L.P. Wakem, F. Sherman, H. Roder, Side chain packing of the N- and C-terminal helices plays a critical role in the kinetics of cytochrome *c* folding, Biochemistry 35 (1996) 5538–5549.
[4] L. Banci, I. Bertini, A. Rosato, G. Varani, Mitochondrial cytochromes *c*: a comparative analysis, J. Biol. Inorg. Chem. 4 (1999) 824–837.
[5] B. Dujon, K. Albermann, M. Aldea, D. Alexandraki, W. Ansorge, J. Arino, V. Benes, C. Bohn, M. Bolotin-Fukuhara, R. Bordonne, J. Boyer, A. Camasses, A. Casamayor, C. Casas, G. Cheret, C. Cziepluch, B. Daignan-Fornier, D.V. Dang, M. de Haan, H. Delius, P. Durand, C. Fairhead, H. Feldmann, L. Gaillon, K. Kleine, et al., The nucleotide sequence of *Saccharomyces cerevisiae* chromosome XV, Nature 387 (1997) 98–102.
[6] M. Nishikimi, S. Ohta, H. Suzuki, T. Tanaka, F. Kikkawa, M. Tanaka, Y. Kagawa, T. Ozawa, Nucleotide sequence of a cDNA encoding the precursor to human cytochrome *c*1, Nucleic Acids Res. 16 (1988) 3577.
[7] R.E. Dickerson, T. Takano, D. Eisenberg, O.B. Kallai, L. Samson, A. Cooper, E. Margoliash, Ferricytochrome *c*. I. General features of the horse and bonito proteins at 2.8 A resolution, J. Biol. Chem. 246 (1971) 1511–1535.
[8] J.A. Knapp, C.N. Pace, Guanidine hydrochloride and acid denaturation of horse, cow, and *Candida krusei* cytochromes *c*, Biochemistry 13 (1974) 1289–1294.
[9] B. Moza, S.H. Qureshi, F. Ahmad, Equilibrium studies of the effect of difference in sequence homology on the mechanism of denaturation of bovine and horse cytochromes-*c*, Biochim. Biophys. Acta 1646 (2003) 49–56.
[10] G. McLendon, M. Smith, Equilibrium and kinetic studies of unfolding of homologous cytochromes *c*, J. Biol. Chem. 253 (1978) 4004–4008.
[11] A. Filosa, A.M. English, Probing local thermal stabilities of bovine, horse, and tuna ferricytochromes *c* at pH 7, J. Biol. Inorg. Chem. 5 (2000) 448–454.
[12] R. Varhac, M. Antalik, M. Bano, Effect of temperature and guanidine hydrochloride on ferrocytochrome *c* at neutral pH, J. Biol. Inorg. Chem. 9 (2004) 12–22.
[13] N. Mirkin, J. Jaconcic, V. Stojanoff, A. Moreno, High resolution X-ray crystallographic structure of bovine heart cytochrome *c* and its application to the design of an electron transfer biosensor, Proteins 70 (2008) 83–92.
[14] P. Chomczynski, N. Sacchi, Single-step method of RNA isolation by acid guanidinium thiocyanate–phenol–chloroform extraction, Anal. Biochem. 162 (1987) 156–159.
[15] E. Margoliash, O.F. Walasek, Cytochrome *c* from vertebrate and invertebrate sources, Methods Enzymol. 10 (1967) 339–348.
[16] D.L. Brautigan, S. Fergusan-Miller, E. Margoliash, Mitochondrial cytochrome *c*: preparation and activity of native and chemically modified cytochrome *c*, Methods Enzymol. 53 (1968) 128–164.
[17] T.Y. Tsong, An acid induced conformational transition of denatured cytochrome *c* in urea and guanidine hydrochloride solutions, Biochemistry 14 (1975) 1542–1547.
[18] E. Margoliash, N. Frohwirt, Spectrum of horse-heart cytochrome *c*, Biochem. J. 71 (1959) 570–572.
[19] F. Ahmad, C.C. Bigelow, Estimation of the free energy of stabilization of ribonuclease A, lysozyme, alpha-lactalbumin, and myoglobin, J. Biol. Chem. 257 (1982) 12935–12938.
[20] P. Emsley, K. Cowtan, Coot: model-building tools for molecular graphics, Acta Crystallogr. D. Biol. Crystallogr. 60 (2004) 2126–2132.
[21] N. Guex, M.C. Peitsch, SWISS-MODEL and the Swiss-PdbViewer: an environment for comparative protein modeling, Electrophoresis 18 (1997) 2714–2723.
[22] R.A. Laskowski, D.S. Moss, J.M. Thornton, Main-chain bond lengths and bond angles in protein structures, J. Mol. Biol. 231 (1993) 1049–1067.
[23] G.N. Ramachandran, V. Sasisekharan, Conformation of polypeptides and proteins, Adv. Protein Chem. 23 (1968) 283–438.
[24] W.L. DeLano, The PyMOL Molecular Graphics System, DeLano Scientific, San Carlos, CA, USA, 2002.
[25] H.W. Chen, S.L. Yu, W.J. Chen, P.C. Yang, C.T. Chien, H.Y. Chou, H.N. Li, K. Peck, C.H. Huang, F.Y. Lin, J.J. Chen, Y.T. Lee, Dynamic changes of gene expression profiles during postnatal development of the heart in mice, Heart 90 (2004) 927–934.
[26] M.M. Santoro, D.W. Bolen, Unfolding free energy changes determined by the linear extrapolation method. 1. Unfolding of phenylmethanesulfonyl alpha-chymotrypsin using different denaturants, Biochemistry 27 (1988) 8063–8068.
[27] S. Taneja, F. Ahmad, Increased thermal stability of proteins in the presence of amino acids, Biochem. J. 303 (Pt 1) (1994) 147–153.
[28] D. Eisenberg, A.D. McLachlan, Solvation energy in protein folding and binding, Nature 319 (1986) 199–203.